Initial publication

Impedance matching and its consequences for modulated electro-hyperthermia

Katja Mühlberg[1], Andras Szasz[2]

[1]Chair of Fundamentals of Electrical Engineering, Technische Universität Dresden, Dresden, Germany
[2]Biotechnics Department, St. Istvan University, Budaors, Hungary

Citation: Mühlberg K. (2021): Impedance matching and its consequences for modulated electro hyperthermia, initial publication: Oncothermia Journal 30: 83 – 104, https://oncotherm.com/sites/oncotherm/files/2021-04/Muhlberg_Impedance_1.pdf

Abstract

This paper demonstrates an opportunity to assess the suitability of an adjustable passive impedance matching network. Various complex impedances shall be transformed to nominal fifty-ohm reference impedance at a given constant carrier frequency. The terminating impedance for optimal matching and gradual mismatching (different degrees of matching) were calculated using mathematics software MATLAB for a matching network's known parameter range. The chosen method, together with the cheap solution, presents a descriptive visualization of the matching network's working principle and resolution capacity. Therefore it can be used as a supporting opportunity for matching network optimization. This network is used for cancer treatment by modulated electro-hyperthermia (mEHT). The accurate matching allows the energy's dosing into the target, which is selected by the body's impedance heterogeneities. The immunogenic effects follow the well-selected energy absorption.

Introduction

Cancer is the number-one deadly disease for humans. Significant efforts and substantial resources are involved in solving this challenge worldwide. A broad spectrum of various approaches exists in treating malignant diseases. Among them, the most known, conventional treatments are surgery, chemotherapy, and radiotherapy [1]. Many additional therapies are emerging to increase the treatment efficacy, elongate survival, and significantly increase the quality of life (QoL) of the suffering patients. One of the complementary methods is hyperthermia, aiming to sensitize or even synergetically increase the conventional therapies' effect. Hyperthermia is usually an isothermal mass heating approach, with the intention of high-temperature activity as a condition to increase the efficacy of the conventional therapies. The majority of heating effects use electrodynamical actions in a non-ionizing regime, and many of them are active in the radiofrequency (RF) range. The technical challenge of these heating processes is optimizing the energy-absorption in depths, focus on the tumor without safety problems; avoid burns on the body's surface or hot-spots inside. In order to solve this problem, modulated electro-hyperthermia (mEHT, trade name oncothermia) was introduced. The mEHT method breaks with the isothermal concept and applies heterogenic selection, targets the malignant cells without direct heating of the tumor's entire mass.

However, this complex cellular manipulation with the applied electric field needs very necessary technical conditions. The crucial point is to direct the energy by impedance matching. In heterogenic heating, the temperature was the usual dose of energy-absorption. The measurability of temperature in the tumor causes many complications. In heterogenic selection, the tumor's temperature cannot be the control parameter; the target's energy absorption decides the dose [2]. The request of the preciosity needs a well-tuned energy-delivery, involving challenges in the technical realization. The objective in this article is to show some parameters of impedance matching in human cancer treatment.

Technical background

The electromagnetic RF energy is capacitively coupled to the body part, when the tumor is located, positioned that the RF-current flows through the cancerous lesion [3]. The carrier frequency is $13.56\ \mathrm{MHz}$ belonging to a radio band that is freely usable for industrial, scientific, and medical (ISM) purposes. The capacitive coupling carefully impedance matched, optimally using the minimal impedance by resonant arrangement. The RF-source is an E-class (switching-mode) amplifier [4]. The patient (which has only a capacitive component in the imaginary part of the impedance) becomes a part of the entire electrical network. Therefore, the patient is considered complex impedance due to the engineering convention being transformed to a $50\ \Omega$ reference impedance by using a passive matching network (tuner). The fixed carrier frequency allows the resonant impedance matching to the load, which is the targeted human tissue.

The system dimensions allow a near-field impedance matching [5]. When the medium impedance changes, a part of the propagated wave is reflected, which has to be minimized. Incoming and reflected waves interfere and create standing waves that represent mismatching. In this case, the system does not completely transfer the available power to the load. However, for cancer patients' mEHT treatment, a continuous and maximum possible power transmission is indispensable to ensure dosage assessment and control. A proper impedance transformer is required to counteract the mismatching that matches the load impedance to the reference impedance. Due to the switching mode resonant amplifier, the correct matching is also a strict request. The patient as the load can have widely different impedances depending on size, muscle and fat content, body hair, origin, treatment location etc., so that a variable impedance transformer with a large latitude of adjustment is necessary. The impedance change during the treatment also could be large enough to correct the matching. The impedance transformer/tuner in mEHT exists and shall be examined for its applicable bandwidth of a broad range of patient impedances. The matching of patient impedances appears as a special challenge; even impedance matching, in general, is a much-discussed topic [6], [7]. However, most of the precise matching fit the fixed antennas, allowing a constant tuning to unchanged impedance. While the patient impedances are multifarious by patients and by treatments, the tuner has to work over a wide range of load parameters.

The compensation of an imaginary part and transforming of a real part to a $50\ \Omega$ reference impedance requires two independent adjustable tuner parameters. The impedance matching during the treatment has to be made dynamically due to constantly changing patient impedances caused by respiration and other physiological changes, including the tumor's change. Therefore, perfect matching cannot be achieved, the tuner has to follow the rough changes and the matching regulation follows a fuzzy logic. In the course of this for the given patient impedance, different tuner parameters constellations can lead to the same degree of matching that is here called as a problem of an ambiguous assignment. This additionally exacerbates the controlling of the tuner. The tuner's optimal matching means that it compensates the impedance of the load ($\underline{Z}_{Load}$) with its impedance regulated ($\underline{Z}_{Tuner}$) impedance, having the $\underline{Z}_0$ reference without imaginary part, Figure 1. [8].

$$\underline{Z}_{Tr} = \underline{Z}_{Tuner} + \underline{Z}_{Load} = \underline{Z}_0 \quad (1)$$

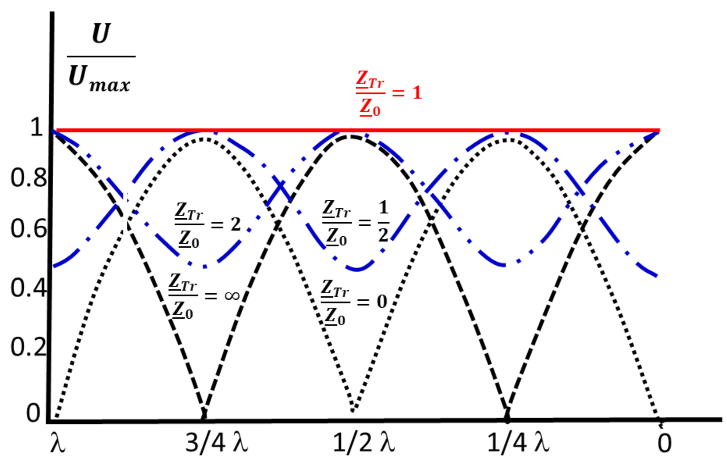

Figure 1. Distribution of the voltage amplitude along the wire versus the matching resistor {Standing Wave Ratio, SWR}, [8]

This paper shows the possible load (patient) impedances for different degrees of matching that were calculated by mathematics software MATLAB [9] with the aid of circuit simulation program "Serenade" [10] for a given adjustable tuner with known parameters range and a constant carrier frequency of $13.56\ \mathrm{MHz}$. The operating principle, together with the resolution of the tuner and the load impedances, in synchrony with their best possible degree of matching, are visualized graphically. Furthermore, the problem of ambiguous assignment of tuner parameter constellations and degree of matching is presented.

The mathematical evaluation of adjustable tuner suitability is a well-illustrative method beneficial for fault finding and optimization of the tuner.

General challenge

Reflections are the consequence of medium impedance changing and can be suppressed by matching each other's impedances. Within an RF circuit, impedance matching has to be considered - generally between source, load, and transmission line. Therefore the common reference impedance $\underline{Z}_0$ of usual $50\,\Omega$ ~~ohm~~ has become established [11] that facilitates the matching by constructing sources and transmission lines with impedance $\underline{Z}_0$. The reference impedance is also referred to as a line, nominal and reference impedance. In the calculation, the E-class resonant RF-source is also fixed to $50\,\Omega$ nominal reference impedance. Figure 2 shows the basic circuit setup for mEHT treatment where the reference impedance is $50\,\Omega$, and the generator delivers the entire power if $50\,\Omega$ transformed load impedance $\underline{Z}_{Tr}$ are connected. The following considerations assume stable reference impedance and carrier frequency.

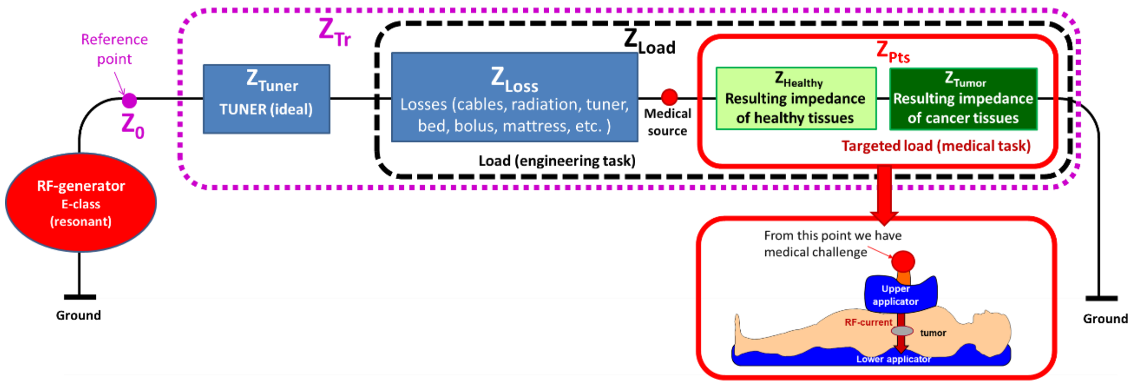

Figure 2. Circuit setup. $\underline{Z}_0$ *reference impedance,* $\underline{Z}_{Load}$ *load impedance,* $\underline{Z}_{Tr}$ *transformed load impedance.* $\underline{Z}_{Tr} = \underline{Z}_{Tuner} + \underline{Z}_{Load}; \underline{Z}_{Load} = \underline{Z}_{Loss} + \underline{Z}_{Pts}; \underline{Z}_{Pts} = \underline{Z}_{Healthy} + \underline{Z}_{Tumor}$

The tuner has a grounding shortcut, so its impedance and the impedance of the complete load is transformed to a parallel ⇔ serial transition. The notes $\underline{Z}_{Tuner}$ and $\underline{Z}_{Load}$ are the transformed impedances.

In complete tuning satisfies:

$$\underline{Z}_{Tr} = \underline{Z}_{Tuner} + \underline{Z}_{Loss} + \underline{Z}_{Healthy} + \underline{Z}_{Tumor} = \underline{Z}_0 \qquad (2)$$

This simply summation works only when the tumor-size corresponds with the electrode size. When it is not the case, the ratio of the $R_{Pts} = \underline{Z}_{Healthy}/\underline{Z}_{Tumor}$ modifies the simple addition. Presently we assume that $R_{Pts} \cong 1$.

This is the engineering task, the reference point, and the nominal $\underline{Z}_0$ reference impedance is to solve the complete tuning, make the engineering task of matching perfectly. The medical task is more complex than the tuning of the hardware; that is, targeting the tumor in depth. The request from the equipment to treat patients is to have perfect tuning (maximize the effect of the RF-generator) and minimize the hardware losses $\underline{Z}_{Tuner} + \underline{Z}_{Loss}$. When the technical request is fulfilled, the task is focused on the patient's net energy source ("medical source"). Consequently, the medical task starts at the applicator on the patient, and the medical challenge is concentrating on the $\underline{Z}_{Tumor}$.

Technical challenge

The occurring wave reflection due to mismatching can be quantified by complex reflection coefficient Γ.

$$\underline{\Gamma} = \frac{\underline{Z}_{Tr} - \underline{Z}_0}{\underline{Z}_{Tr} + \underline{Z}_0} \tag{3}$$

Its absolute value can lie between 0 and 1, where 0 means perfect matching. In the case of reflection incident and reflected wave interfer and create standing waves. The voltage standing wave ratio $VSWR$ describes the ratio between the maximum and minimum voltage of standing voltage wave. It can also be calculated using the reflection coefficient.

$$VSWR = \frac{1 + |\Gamma|}{1 - |\Gamma|} \tag{4}$$

$VSWR$ attains values of 1 and higher where 1.0 corresponds to perfect matching. The amount of power loss caused by reflections is expressed by return loss RL that describes the ratio between incident P_i and reflected power P_r and can also be gained from $VSWR$.

$$RL = 10\ \log_{10}\left(\frac{P_i}{P_r}\right) \tag{5}$$

$$RL = -20\ \log_{10}\left(\frac{VSWR - 1}{VSWR + 1}\right) \tag{6}$$

By equating formula (5) and (6), the ratio between reflected and incident power can be calculated:

$$\frac{P_r}{P_i} = \left(\frac{VSWR - 1}{VSWR + 1}\right)^2 = |\Gamma|^2 \tag{7}$$

An example: let us calculate when the reference impedance $\underline{Z}_0 = 50\ \Omega$ and load impedance is transformed to $\underline{Z}_{Tr} = (60 - j10)\ \Omega$. In this case, we receive the reflected power of about $1.6\ \%$, taking the reflection coefficient from (3) and the subsequent ratio between reflected and incident power from (7). The task is to minimize |Γ| and the $VSWR$.

The transformation of complex load/patient impedance requires two independent adjustable tuner parameters C_1 and C_2. The transformed load impedance $\underline{Z}_{Tr}$ depends therefore on three parameters – the two tuner parameters and the load. The reference impedance of $\underline{Z}_0 = 50\ \Omega$ together with $\underline{Z}_{Tr}$ determine the $VSWR$ value. The relations in general:

$$\underline{Z}_{Tr} = f(\underline{Z}_0, VSWR) \tag{8}$$

$$\underline{Z}_{Tr} = f(\underline{Z}_{Load}, C_1, C_2)\ \leftrightarrow\ \underline{Z}_{Load} = f(\underline{Z}_{Tr}, C_1, C_2) \tag{9}$$

From (3) and (4) the perfect matching ($VSWR = 1.0$) can only be achieved if $\underline{Z}_{Tr}$ equals $\underline{Z}_0$. Every possible constellation of tuner parameters and deduced $\underline{Z}_{Tr}$ can be calculated in the perfect matching. However, in mismatching ($VSWR > 1.0$) the calculation of load impedance becomes more complicated. Like (4) shows, only the absolute value of the reflection coefficient (|Γ|) is of interest to calculate the $VSWR$. The challenge happen realizing that the different $\underline{Z}_{Tr}$ values can cause the same |Γ|. Therefore it is not possible to calculate the transformed load impedance $\underline{Z}_{Tr}$ in case of $VSWR > 1.0$. The relation between $VSWR$ value and transformed load impedance $\underline{Z}_{Tr}$ forms ring structures (Fig. 3.), allow the arbitrary direction of $\underline{Z}_{Tr}$ vectors keeping the absolute value ($\underline{Z}_{Tr} = \underline{Z}_0 + \underline{Z}_r$) where $|\underline{Z}_r|$ is the radius of the circles in Fig. *3.* determined by a constant $VSWR > 1.0$.

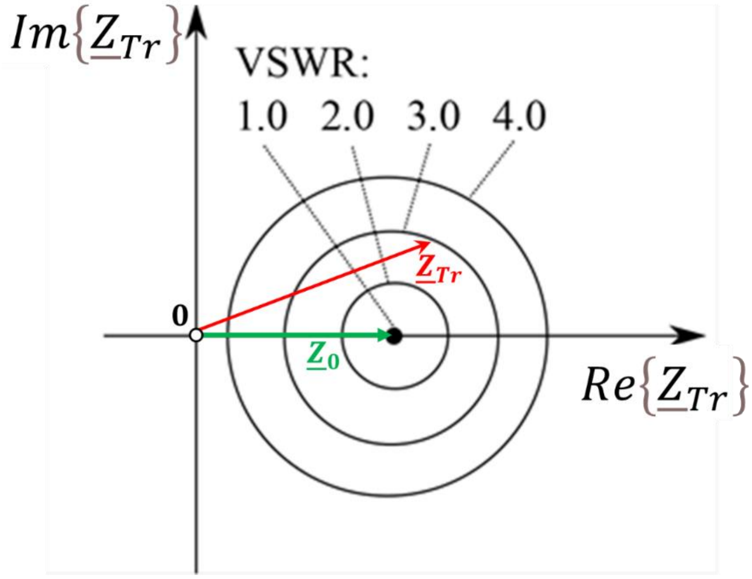

Figure 3. The relation between $VSWR$ and transformed load impedance $\underline{Z}_{Tr}$. The actually shown transformed load is realized at $VSWR = 3$.

The middle point on Fig. *3.* shows the clear assignment between $\underline{Z}_{Tr}$ and $VSWR$ values when $VSWR \equiv 1.0$. For $VSWR > 1.0$ the $|\underline{Z}_{Tr}|$ has to be determined first. The tuning challenge is huge due to the $Im\{\underline{Z}_{Tr}\}$ could be extremely large, while the shrinking real-part tends to $\underline{Z}_{Tr} = \underline{Z}_0$, when $Im\{\underline{Z}_{Tr}\} = 0$. Consequently, the load impedance in the circle has to be calculated for every constellation of tuner parameters. Note that $\underline{Z}_{Tr}$ values are in pairs of positive or negative admittance at the same $|\underline{Z}_{Tr}|$. Introducing the parameter $VSWR_{x\_circ}$ describes the circle function on the corresponding set of impedances $\underline{Z}_{Tr}$ causing a $VSWR$ of value x. In contrast to that $VSWR_{x\_area}$ characterizes that area that includes all load impedances $\underline{Z}_{Load}$ which can be transformed to a minimal $VSWR$ of value x (best possible, optimal matching).

Based on the ultimate trans-match model [12], the tuner circuit could be realized like it is a circuit shown in Fig. 4. The L is the constant coil inductivity and C_1 and C_2 are adjustable rotary capacitors. Capacity C_1 consists of two identical condensers controlled symmetrically, while C_2 is independent. Consequently, two separate parameters define the tuning by individual control of the tho capacitive components. In calculation, we use a resolution of 100 steps for each. The existence of the two parameters corresponds to the real and imaginary parts of the matching. The number of the parameters defines the angle of $\underline{Z}_{Tr}$ by the vector components in the circle of radius $|\underline{Z}_{Tr}|$ when $VSWR > 1.0$.

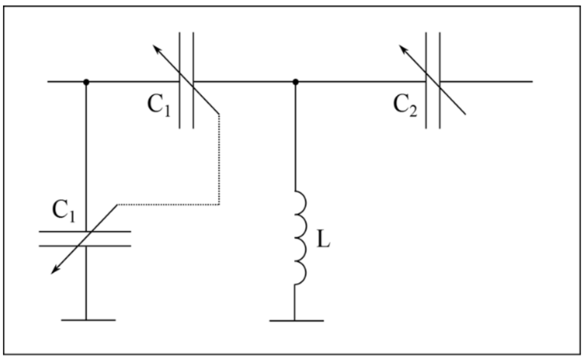

Figure 4. Tuner circuit with adjustable capacitors C_1 and C_2 and constant coil inductivity L.

The transformed load impedance $\underline{Z}_{Tr}$ can be calculated using figures 2 and 4. Thus the load impedance $\underline{Z}_{Load}$ at constant carrier frequency f_c is

$$\underline{Z}_{Load} = \frac{1}{\frac{1}{\frac{1}{\frac{1}{\underline{Z}_{Tr}} - j\omega C_1} - \frac{1}{j\omega C_1}} - \frac{1}{j\omega L}} - \frac{1}{j\omega C_2} \quad (10)$$

where

$$\omega = 2\pi f_c \quad (11)$$

First, the transformed load impedances $\underline{Z}_{Tr}$ for the specified $VSWR$ value has to be found. In full matching $\underline{Z}_{Tr} = \underline{Z}_0$. Consequently, when the system is well-tuned ($VSWR = 1.0$; $\underline{Z}_{Tr} = \underline{Z}_0$), the load can be calculated:

$$\underline{Z}_{Load} = \frac{\frac{j\omega LC_1\underline{Z}_0}{C_2} + \frac{2\underline{Z}_0}{j\omega C_1} + j\omega 2\underline{Z}_0 L - \frac{L}{C_2} + \frac{1}{\omega^2 C_1 C_2} - \frac{L}{C_1}}{j\omega L + \frac{1}{j\omega C_1} + \omega^2 \underline{Z}_0 L C_1 - 2\underline{Z}_0} \quad (12)$$

(Conventionally $\underline{Z}_0 = 50\ \Omega$, so we use this value for model-calculations.)

After that, all load impedances for all constellations of tuner parameters C_1, C_2 and equally distributed and quantitatively satisfactory $\underline{Z}_{Tr}$ on the $VSWR_{x\_circ}$ the circle can be calculated. The result of that depends on the amount of $\underline{Z}_{Tr}$ points numerous single impedance areas (for each $\underline{Z}_{Tr}$ point one area) that are overlapping and evolve the entire area – the $VSWR_{x\_area}$. From the gathered impedance points extracted from the border of $VSWR_{x\_area}$. The density of impedance points in the area gives information about the resolution of the tuner and with known C_1, C_2 and L values for a specific $\underline{Z}_{Tr}$ the operating principle of the tuner can be comprehended. This information is also used to visualize the ambiguous assignment of tuner parameter constellations and the degree of matching.

With the aid of the circuit simulation program "Serenade" the $VSWR_{x\_circ}$ functions were interpolated. The tuner circuit shown in figure 4 and complex load impedance were implemented, and the reference impedance of $50\ \Omega$ and the carrier frequency of $13.56\ \mathrm{MHz}$ defined. Furthermore the constants and adjustable parameters with their ranges in the tuner were set. For six different complex user-defined load impedances $\underline{Z}_{Load}$ and the determined goal $VSWR$ value the C_1, C_2 constellations were simulated. For each gathered $\underline{Z}_{Load}$, C_1, C_2 constellation the transformed load impedance $\underline{Z}_{Tr}$ was calculated. All six single simulations had the same goal $VSWR$ of value x so that the resulting $\underline{Z}_{Tr}$ points drawn in complex plane lay on the $VSWR_{x\_circ}$ circle. By method of least squares using Gauss-Newton algorithm, the circle was interpolated and its function with radius r, real axis shift m_1 and imaginary axis shift m_2 be extracted.

$$r^2 = (x - m_1)^2 + (y - m_2)^2 \quad (13)$$

The circle function can also be expressed by polar coordinates where φ describes the angle between $\underline{Z}_{Tr}$ impedance vector and real axis counterclockwise.

$$x = m_1 + r \cdot \cos\varphi \quad (14)$$

$$y = m_2 + r \cdot \sin\varphi$$

In $3.6°$ steps, the coordinates of 100 equally distributed and quantitatively satisfactory $\underline{Z}_{Tr}$ points per circle were obtained. The number of $\underline{Z}_{Tr}$ points is freely selectable, whereby a higher number of points provides a finer border of the calculated entire impedance area.

In ideal conditions the $VSWR = 1$, and the possible $\underline{Z}_{Load}$ impedances have a large set of values. For perfect matching $\underline{Z}_{Tr}$ has to equal $\underline{Z}_0$ that is assumed to be constant $50\ \Omega$. Therefore the load impedance is $\underline{Z}_{Load}$. It depends only on the two adjustable capacitors C_1 and C_2: $\underline{Z}_{Load} = f(C_1, C_2)$. For 100 C_1 and 100 C_2 values the load impedances $\underline{Z}_{Load}$ can attain 10000 impedance points shown in a complex plane below. The different adjusting of tuner capacitors and their resulting changing of load impedance $\underline{Z}_{Load}$ is marked Fig. 5. This means that all of these loads could be ideally matched with $VSWR_{1.0\_area}$.

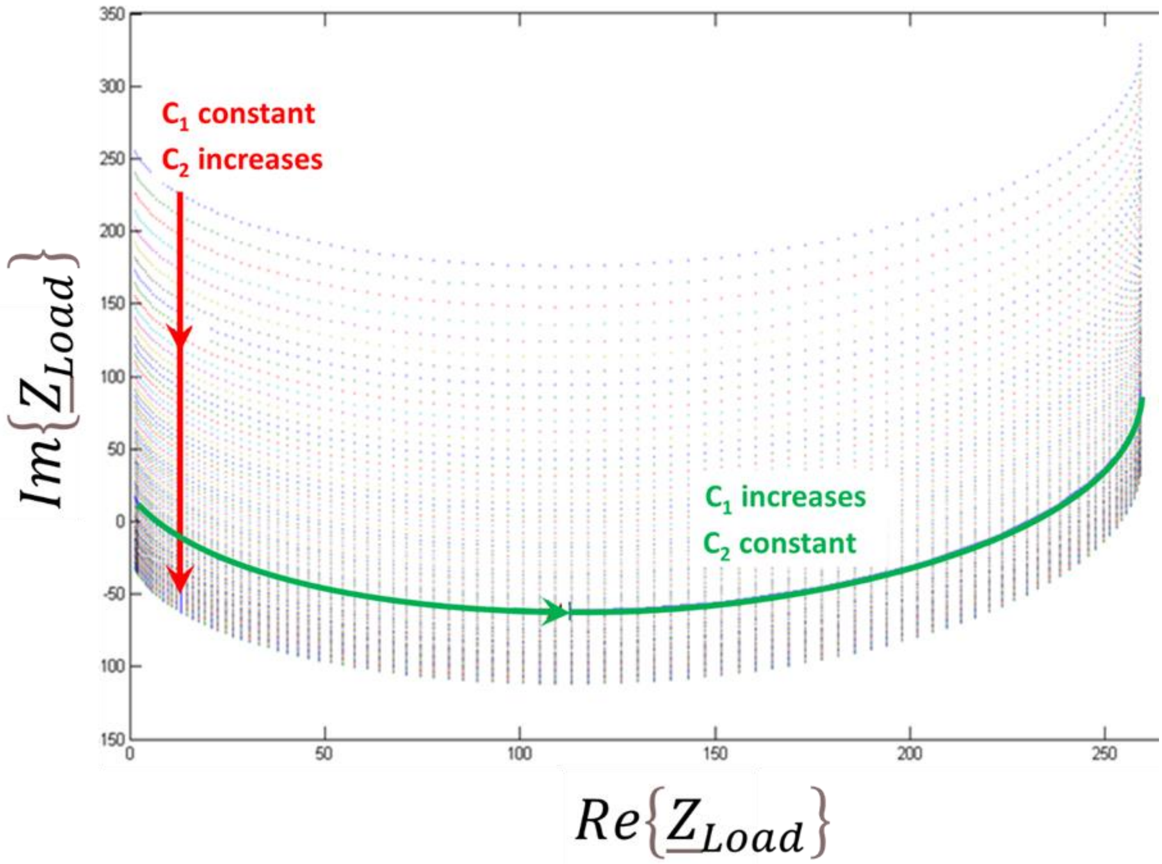

Fig. 5. The complex $\underline{Z}_{Load}$ at $VSWR_{1.0\_area}$. The load impedance $\underline{Z}_{Load}$ depends on the transformed load impedance $\underline{Z}_{Tr}$ and the two adjustable capacitors C_1 and C_2: $\underline{Z}_{Load} = f(\underline{Z}_{Tr}, C_1, C_2)$.

When $VSWR$>1, then the reference points form a circle in the actual calculation as expected by Figure 3. For a defined step size of φ the x and y values (resistances and reactances) of reference points could be generated (Figure 6.). Subsequently, their impedance areas are calculated. The contour points were detected and collected. The last step was evaluating the contour of the single contour points representing the border of the specified VSWR area.

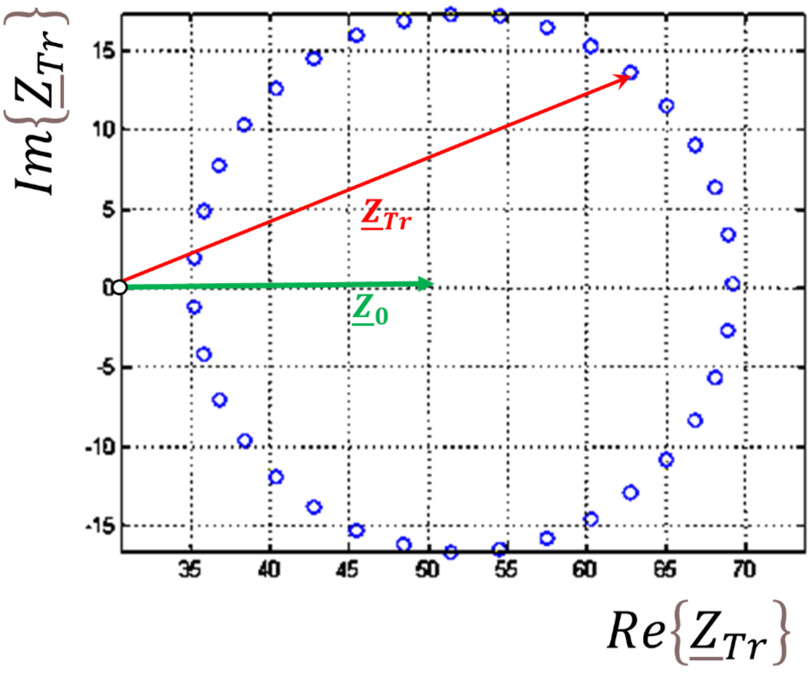

Figure 6. 36 reference points for $VSWR = 1.4$. An arbitrary $\underline{Z}_{Tr}$ is shown.

For suboptimal degrees of matching like $VSWR = 1.4$, the load impedance $\underline{Z}_{\mathrm{Load}}$ depends not only on the capacitor values C_1 and C_2 but also on the transformed load impedance $\underline{Z}_{\mathrm{Tr}}$, $\underline{Z}_{\mathrm{Load}} = f(\underline{Z}_{\mathrm{Tr}}, C_1, C_2)$ (Figure 7.). The transformed load impedance $\underline{Z}_{\mathrm{Tr}}$ can actually attain infinite values laying on an impedance circle corresponding to the specified VSWR value. Therefore infinite single load impedance areas result.

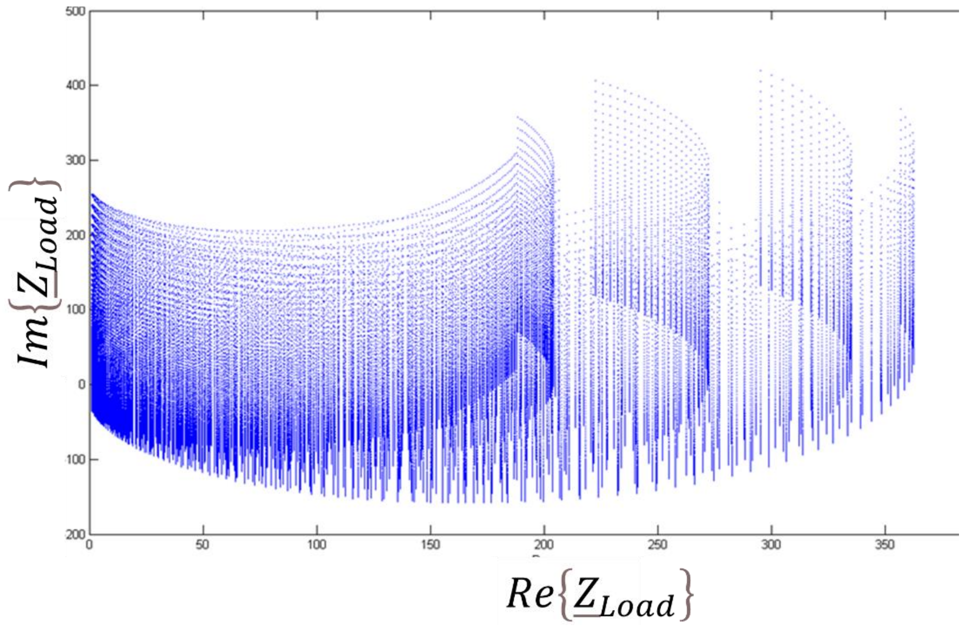

Figure 7. The $VSWR_{1.4\_area}$ no perfect matching Every tenth single area from 100 calculated. Every single load impedance area was calculated for 10000 different C_1, C_2 constellations.

The single impedance areas create an entire impedance area that border was detected for the specified $VSWR$ value in Figure 8.

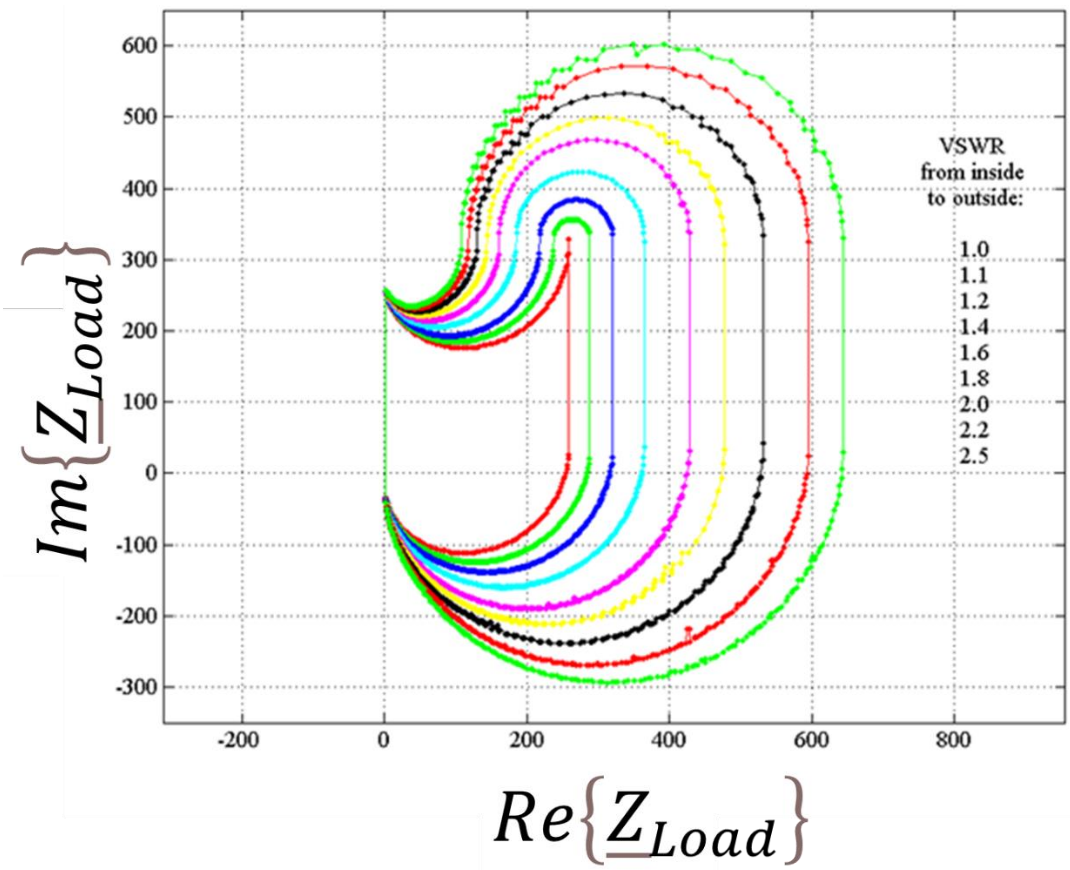

Figure 8. The borders of entire load impedance areas for chosen $VSWR$ values.

The calculated impedance area for perfect matching from figure 5 is related to capacitor values C_1 and C_2. In this case the single impedance area corresponds to the entire impedance area because the transformed impedance load $\underline{Z}_{Tr}$ has to equal the reference impedance of constant $50\ \Omega$, Figure 9.

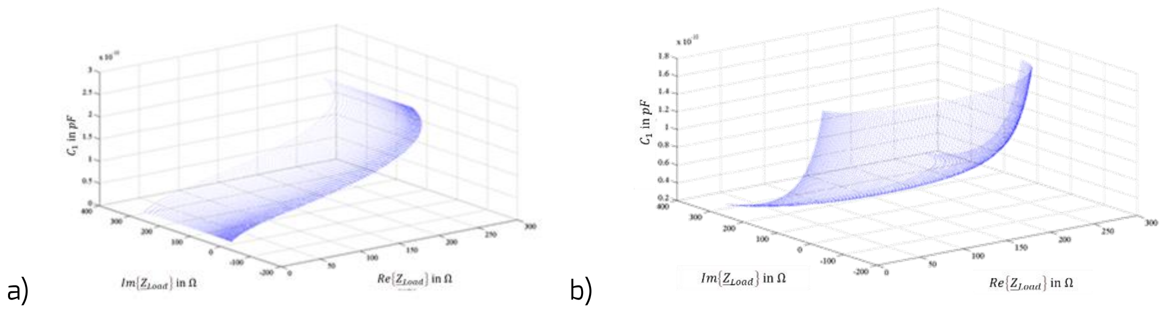

Figure 9. C_1 and C_2 dependence on $VSWR_{1.0\_area}$.

The calculated single impedance areas from figure 7 are shown with their related C_1 and C_2 values. However, the load impedances not only depend on the adjustable capacitor values C_1, C_2 but also on the transformed load impedance $\underline{Z}_{Tr}$. The overlapping single impedance areas plotted above form a volume, implying that the same load impedance $\underline{Z}_{Load}$ can be tuned to a specified VSWR value greater than one by different C_1, C_2 constellations *Figure 10.*

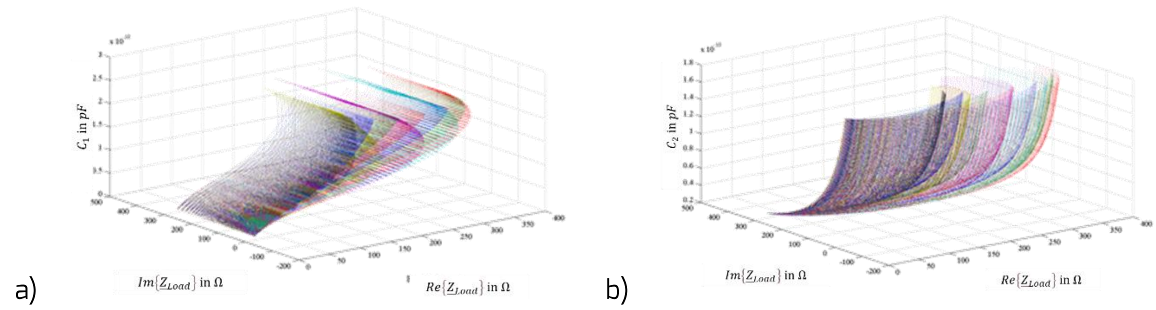

Figure 10. C_1 and C_2 dependence on $VSWR_{1.4\_area}$.

The different density of load impedance points in figure 5 delivers two statements. The first is that the tuner sensitivity is different within the impedance area. Load impedances within this area with very low or high real part or low imaginary part can be tuned finer in general than impedances with the high imaginary part. This leads to the second statement that an extension of tuner parameter range has only effect graphically seen for the upper border of impedance area by adding lower C_2 values. In contrast to that, all other possible range extensions of C_1 and C_2 do not enlarge the area due to the increasing density of points towards the borders. If a higher resolution within the impedance area for perfect matching is desired the C_1 and C_2 steps have to be minimized.

As expected does a lower degree of matching results in a larger load impedance area indicated by figure 7. However, the area extension is not symmetrical in all directions that, due to non-existing impedances with the negative real part, is comprehensible. Partly an overlapping of single impedance areas is shown that indicates that two possible C_1, C_2 constellations for one load impedance $\underline{Z}_{Load}$ lead to the same transformed load impedance $\underline{Z}_{Tr}$.

The plotted borders for chosen $VSWR_{x\_area}$ in figure 8. show, that generally, load impedances with high real and low absolute imaginary part are more straightforward to match than those with low real part and high absolute imaginary part.

Considering the problem of ambiguous assignment of tuner parameters and degree of matching so can be said that for a perfect matching in figure 9 every load impedance in this area has exactly one C_1, C_2 constellation and unique assignment prevail. In contrast to that figure 10 shows the C_1 and C_2 dependence for a worse degree of matching. A specified load impedance in the $VSWR_{>1.0\_area}$ area can be transformed by different C_1, C_2 constellations and the assignment is not unique anymore. For worse degrees of matching this problem intensifies. The problem can be seen from another direction. For a measured $VSWR$ value and known C_1, C_2 values obtained from step motors positions the load impedance $\underline{Z}_{Load}$ cannot be determined that exacerbates the controlling of the tuner. It shall be pointed out again that all considerations suppose stable reference impedance and carrier frequency.

Technically essential to solving that the $\underline{Z}_{Tuner}$ is minimal when matches the $\underline{Z}_{Load}$ to the $\underline{Z}_0$ reference. Other technical challenges are connected to the minimalization of the$\underline{Z}_{Loss}$

Medical challenge

The complex medical task starts at the applicators, which are included in the medical task as an important energy transmitter, constructed for human physiology, ergonomy, and medical practice, see Fig. 11. On the other hand, the applicator has technical tasks also. The impedance matching sharply depends on how the transmitting electrodes are connected to the human body.

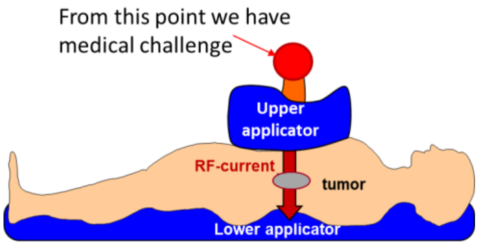

Figure 11. The RF-current flows through the body. The medical challenge starts at the applicators.

Important behavior of the applicators is the perfect shape adaptation avoiding the high impedance of the transmission. The carefully selected materials and structure of the applicators minimize the losses. The broad range of electromagnetic heterogeneity of the body is the next barrier Fig. 12. The only easing of the challenge is the missing inductive factor in the body, so the impedance of tissues has only negative reactance.

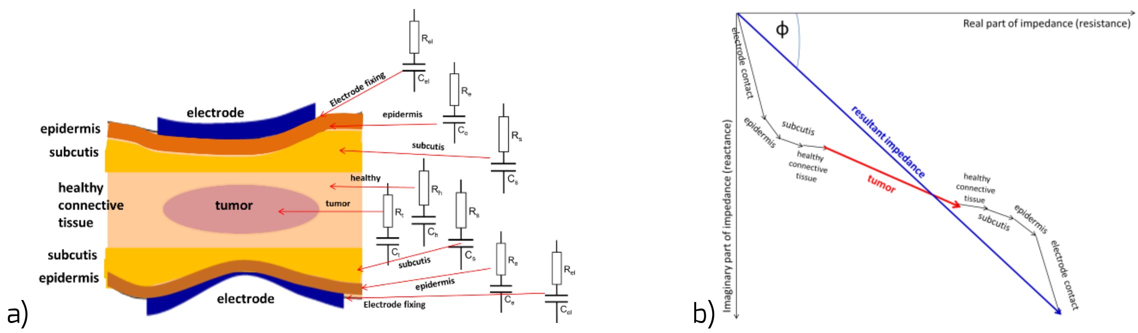

Fig. 12. The main, macroscopic electromagnetic heterogeneities of the body. (a) The layer structure (the essential micro-heterogeneities of the various tissues are not shown.) (b) The resultant impedance vector (Only some macro-heterogeneities are shown for clarity.)

However, in capacitive coupling on a larger volume (like belly, chest), Eddy-current could generate a slight induction, as shown in Figure 13.

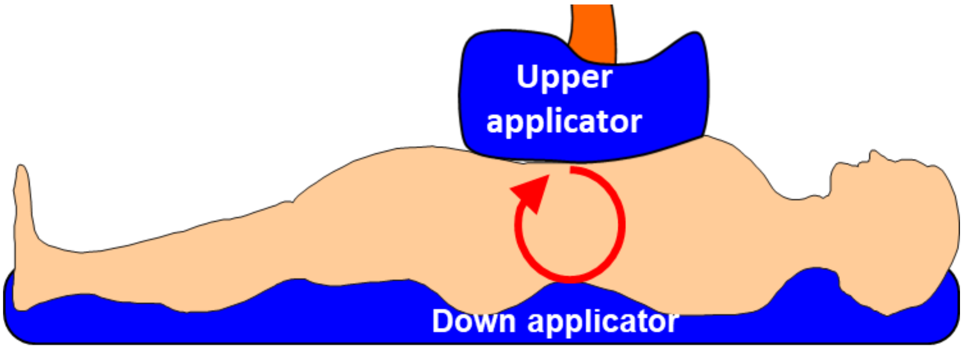

Figure 13. The induced Eddy current in a large part of the body by RF capacitive coupling. (It depends, of course, on the frequency, the current conduction, and sizes of the body-part.

Measurements in various healthy human volunteers show this tendency in Figure 14. The possible Eddy current inductivity in the belly significantly differs from other body-parts.

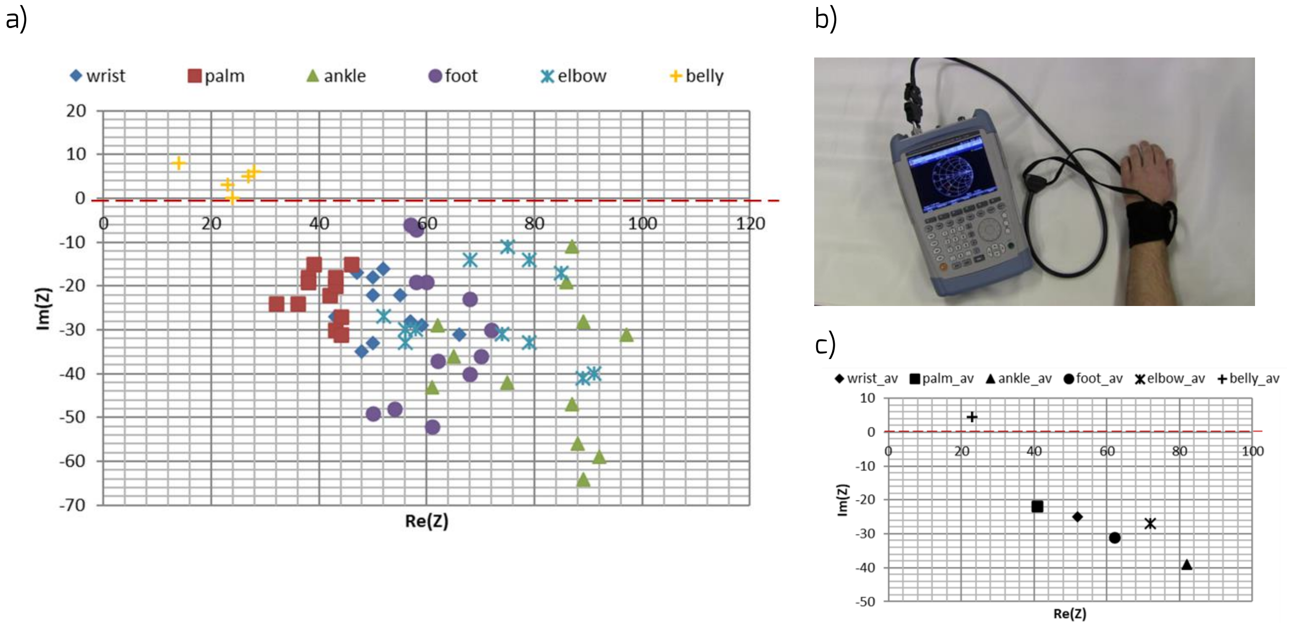

Figure 14. Impedance measurements on human volunteers with capacitively coupled different plan-parallel electrode sizes fit the size of the body-part. (a) the results depend on the person. (b) example of the wrist measurement. (c) The black markers show the averages.

The technical solution has to serve the medical task to provide optimal energy in the tumor considering the broad range of the individual variation of the impedances. This task is a considerable challenge that needs technical and physiological, biophysical, and medical considerations. The solution could be the mEHT, which is designed to handle all the demanding details.

The mEHT method is one part of the cancer therapies. The treatment goal is to deliver energy absorbed at the tumor-cells and start the antitumor-effect by eliminating the selected cells and liberating their genetic information to form an antigen-presenting process developing a tumor-specific immune-reaction by in-situ effects, without ex-body laboratory manipulation [13].

The massive micro and macro heterogeneity of the living tissues block the isothermal heating, but it allows the selection. The selection uses the bioelectromagnetic, thermal, and structural peculiarities of the malignant cells and their microenvironment (mE) [14]. The guiding selection factor are the impedance differences between the malignant and healthy cells [15]. The real part of the impedance is strongly influenced by the cells' ionic content and their mE. The malignant cells mostly metabolize much more intensively, which is measurable by positron emission tomography (PET). This shows the extreme glucose demand of the tumor, producing ATP in a fermentative way. This mode of ATP production is speedy and straightforward but considerably less effective than the standard Krebs-cycle in mitochondria [16]. The mitochondria function is suppressed, and it is stated as the primary cause of cancer [17]. Due to their huge energy-demand for cellular reproduction, so the ionic component around them well differs from their host. The imaginary part of the mE is determined by the missing (or damaged) networking of malignant cells. The cancer cells are mostly autonomous. They are individual, separated "fighters" for the energy to survive. This autonomy changes their mE, the missing cellular connections, and the disordered structure of aqueous electrolyte around them will increase the relative dielectric constant (ε_r) of the mE region. The disorder is mE "dismantles of multicellularity" [18]. The impedance drastically changes by the higher conductivity and higher dielectric constant than standard. The two effects support each other [19], and RF current flow recognizes it due to the noticeable changes.

The application of bioelectromagnetic differentiation in biological tissues attracts the attention of researchers [20]. Various publications show considerable differences between the impedance parameters of malignant tissues from their healthy hosts. The current density image by MRI (RF-CDI) well visualizes the increase of the RF-current density in tumors [21]. The in vivo measurements show that the necrotic cell-destruction approx. linearly depends on the conductivity in the range of $10\text{ Hz} - 1\text{ MHz}$ [22]. (24 tumors of the $K12/TRb$ rat colon cancer.) The conductivity of $VX-2$ carcinoma and normal rabbit liver tissues ex-vivo also shows the differences [23]. The impedance variation shows good resolution of tumor-in the mice by control comparison with MRI [24]. In human measurements with coaxial line sensor, the heterogeneity well proven in ductal and lobular tumors compare them to the surrounding tissues in $0.02 - 100\text{ MHz}$ range [25]. The breast tissues were very intensively examined to replace the ionizing radiation in mammography with more safe electromagnetic tomography [26], [27]. The water content of the tissue also has considerable addition to the electric behavior of tumor [28]; which makes extra selection factor due to the water content is significantly higher in the tumor than its host. Furthermore, the extracellular fluids in mE form bound water, which has larger values of σ and ε than free water. Pleasant help, that the Debeye model comparable with the measurements [29], and when it modified, the similar Cole-Cole model describes the situation [30]:

$$\text{Debeye:} \qquad \varepsilon^*(\omega) = \varepsilon_\infty + \frac{\varepsilon_s - \varepsilon_\infty}{1+i\omega\tau}$$

$$\text{Cole-Cole:} \qquad \varepsilon^*(\omega) = \varepsilon_\infty + \frac{\varepsilon_s - \varepsilon_\infty}{(1+i\omega\tau)^{1-\alpha}} \qquad (15)$$

The Cole-Cole model well approximates the heterogenic changes like organelles, cellular edemas, ischemic tissues, gap-junctions, etc. [31] by deformation of the clear semicircular shape. The Cole-Cole formulation well demonstrates the importance of the electromagnetic heterogeneities in the target [32]. The conduction differences in the micro-range also used against pathogens in food-processing [33]. For example, the frequency dependence of energy absorption by insects used against rice weevil [34].

The heterogeneity affects the relaxational processes in a broad spectrum of frequencies [35]. However, the frequency dispersion modifies different parts of the tissue and cells, and gives a possibility for further selection by low frequency ($\alpha - dispersion$), radio frequency ($\beta\ \&\ \delta - dispersions$), and microwave frequency ($\gamma - dispersion$) processes [36]. The usefulness of the 13.56 MHz is not only because it is a part of the medically allowed ISM frequencies, but also because its geometrical selectivity [37], as well as its special position in the boundary of the $\beta\ \&\ \delta - dispersions$.

The $\beta - dispersion$ targets the membrane-electrolyte structures of cells, performing Maxwell-Wagner relaxation [38]. The interfacial polarization of the cell membranes [39], consequently, the charge distribution at the cellular of interfacial boundaries [40] play a central role in the process. The charge buildup causes the characteristic variation of the $\beta - dispersion$ [41]. A transition occurs from $\alpha - dispersion$ to $\beta - dispersion$ in ex-vivo haddock muscle [42] a few hours after its removal from the fish. It was increased in the same period of time, according to The different tissue decomposition process mechanisms causing the change in this frequency range. The upper-frequency boundary of $\beta - dispersion$ has additional peculiarity usually noted as $\beta 1 -$

$dispersion$. The torque of biological macromolecules caused by the proteins keeping their orientation against the disordering electromagnetic effects form large dipole moments, which do not follow the high-frequency changes [43]. The vast heterogeneity of the biological tissues causes multiple effects on the excited molecules, like the conformational change of the polymers [44], the macromolecular relaxation interaction with the ionic effect in the vicinity of them [45].

The $\delta - dispersion$ is just overlapping the high-frequency end of the $\beta - dispersion$ [46]. The dipolar moments of proteins and other large molecules (like cellular organelles, biopolymers) distinguish this frequency interval [47]. It is a second Maxwell-Wagner dispersion (δ) act on suspended particles, diffusion of charged molecules surrounded by a cell [48], near membrane bounds completed with protein-bound water, and cell organelles such as mitochondria [49], [50]. Electromagnetic selection of the malignant cells guides the energy delivery. The $\beta/\delta - dispersion$ of the carrier frequency allows to distinguish the variance of the impedance of these cells [51], orients the attack on the membrane reaction of the impedance selected cells [52], [53], primarily for the groups of transmembrane proteins [54], [55], [56]. The $13.56\ \mathrm{MHz}$ lies inside the $\beta/\delta - dispersion$, so it offers a natural choice for medical electromagnetic applications [57]. The selection was shown on molecular levels, too [58], [59]. Importantly the bound water on the membranes and proteins also has a special absorption increase in the $10\ \mathrm{MHz}$ range [60]. The applied electromagnetic treatment synergically applies the field-effect together with the increased temperature by the absorbed energy [61], depending a lot of biophysical interactions in the microenvironment of the targeted cell [62]. The plasma membranes' heterogeneity has various origins, but the decisional is a mixture of transmembrane membrane proteins with membrane-lipids, forming clusters, called lipid rafts. Many molecular and physiological processes are determined by the heterogeneous lipid domains serving as molecular sorting platforms [63]. The malignant cells have a denser lipid-raft population on their membranes than their healthy counterparts [64]. Consequently, membrane heterogeneity has a crucial role in the selective energy-absorption of malignant cells - see Figure 15.

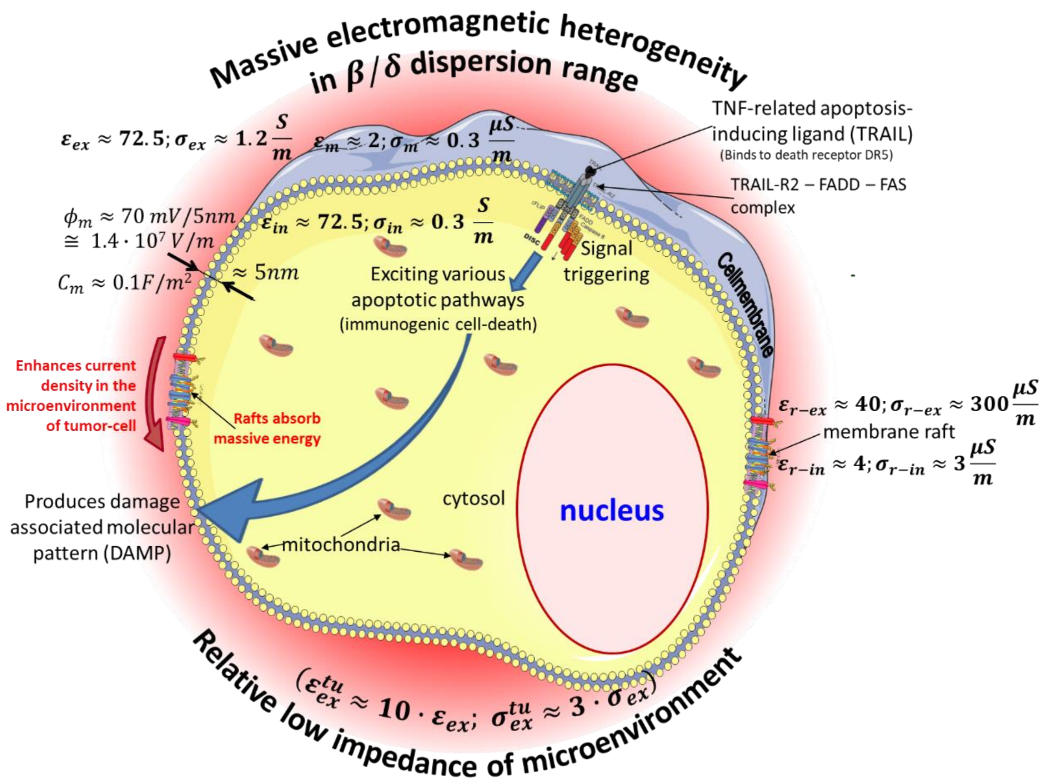

Figure 15. The electromagnetic heterogeneity of the selected tumor-cell as a target of the $\beta/\delta - dispersion$. Abrevations/references: ε_{ex} and σ_{ex} are the relative permittivity and conductivity of extracellular electrolyte in the microenvironment of a cell [65]; ε_{ex}^{tu} and σ_{ex}^{tu} are the relative permittivity and conductivity of extracellular electrolyte in the microenvironment of a tumor cell [27]; : ε_m and σ_m are the relative permittivity and conductivity of the cell-membrane [66] ; ε_{in} and σ_{in} are the relative

permittivity and conductivity of intracellular electrolyte of a cell [65]; ε_{r-in} and σ_{r-in} are the relative permittivity and conductivity of intracellular side of raft proteins [67],[68];ε_{r-ex} and σ_{r-ex} are the relative permittivity and conductivity of extracellular side of raft proteins [69],[70]. The apoptotic way is shown by various publications [71], [72], [73].

The membrane structure may drastically change by variation of temperature producing a phase-transition of the configuration [74]. The membrane goes through a Gel/Sol transition from a denser to a more fluid state at a defined temperature. The rearranged packing of unsaturated phospholipids results from a higher fluidity [75]. The transition decision involves the lipid rafts [76]. Note that the well-known break on the Arrhenius plot [77] could be formed by phase transition [78].

The phase transition is not as simple in living conditions as happens in most non-living situations. The conditions of living reactions governed by various enzymes which catalyze and ease the transition, lowering the usual energy-gap between the reactants (A_1) and products (A_2). The transition-state theory involves quantum-mechanical considerations [79], [80], [81] to describe the excited enzymatic state (A^*), allowing tunneling to avoid the energy to jump through the high peak [82] (Figure 16.). The complex A^* state could have direct jump into final products A_2 with unidirectional transition probability k_3. However, the complex A^* state is unstable in the backward direction with k_2 transition probability:

$$A_1 \underset{k_2}{\overset{k_1}{\rightleftarrows}} A^* \overset{k_3}{\rightarrow} A_2 \tag{16}$$

The enzymatic process has a "point of no return", when the reversing of the transition became impossible. This interdisciplinary approach [83] explains the experiment-based classical Arrhenius law. In case of increasing temperature like hyperthermia requests it, this phase-transition process determines the structures [84], which were later verified independently, [85], [86].

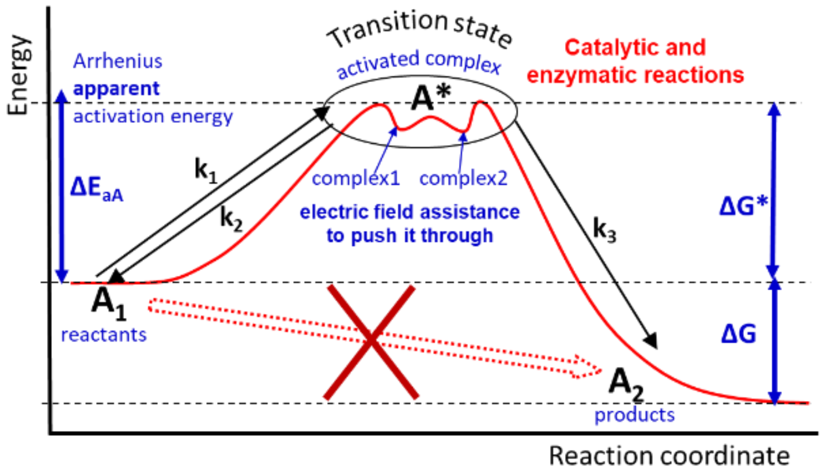

Figure 16. The direct transition between A_1 and A_2 is impossible due to the energy barrier. The height of the barrier was lowered by enzymes and also by the electric field-assisted transition. The A^* transition state is a complex molecular reaction, and the field pushes it to the point of no return to finish the transition process.

The transition state could be created by electromagnetic reactions (or its reaction complexes with molecules); the temperature effects have certain similarities with electric field action [87].

The main step of the energy targeting is the selective absorption on the transmembrane proteins, which is surrounded by the isolating lipid-bilayer of the membrane material [88]. The clustered transmembrane proteins (membrane rafts) absorb the energy, which is shown by model calculation too [89]. The malignant cells follow dominantly apoptotic way of death [90] in mEHT. The absorbed energy by transmembrane proteins ignites particular signal-pathways to promote the programmed cell-death (apoptosis) [91], which could happen with a synergy of conventional chemotherapies [92]. Molecular investigation shows the significant difference between conventional heating and mEHT [93], [94]. The missing homeostatic harmony in cancer is also a selective factor. Modulation is applied to recognize the homeostasis spectrum, selecting the nonharmonic parts of the target [95]. The amplitude modulation (AM, $< 20\,\mathrm{kHz}$) of the RF carrier frequency intensifies the tumor-specific absorption [96]. Despite the small energy absorption [97], the membrane demodulates the signal and causes damages in the cytosol [98]. The complex action of mEHT well synergizes the "thermal" and "nonthermal" effects [99], with high selective preciosity [51]. The "gentle" elimination process allows liberating the genetic information of the malignant cells by developing damage-associated molecular pattern (DAMP) [100]. The energy absorption triggers immune effects by specific apoptosis, the immunogenic cell-death (ICD) [101], [102]. The transferred genetic info allows maturating antigen-presenting cells (APCs) to produce helper and killer T-cells for systemic antitumor effect on micro and macrometastases (abscopal effect) [13], [103]. In this way, the local treatment could be extended systematically to the entire body when the tumor-specific immune reaction develops, killing CD8+ T-cells prepared by the antigen information from cancer cells by ICD, [104], Fig. 17. The systemic (abscopal) effect is proven in preclinical [105], and in clinical applications [106]. This process well fits the trend of the development [107].

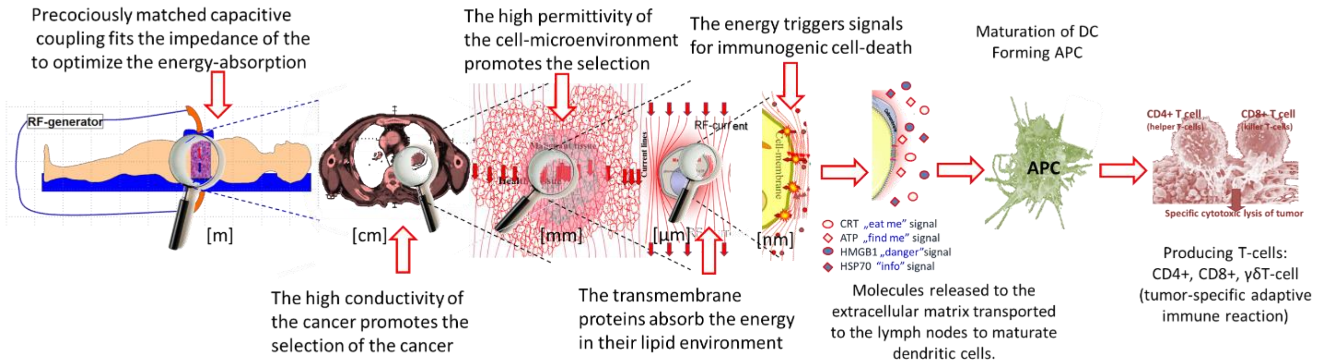

Fig. 17. The mEHT method has a series of effects. The first step is the accurate matching for energy-control, and then the impedance differences make the selection. The hyperthermic step happens when the membrane raft absorbs the energy. In consequence, a set of signals to death is triggered (immunogenic cell-death), which prepares antigen-presenting possibility, forming tumor-specific immune reaction.

Conclusion

The proper oncological hyperthermia needs high-preciosity matching and target-selected energy-absorption. Its resolution capacity, the load impedances for a given degree of matching, the effect of tuner parameter adjusting, and the problem of ambiguous assignment of tuner parameters and degree of matching were visualized. Thereby the conceivable extension of tuner parameter ranges and their optimization limits could be demonstrated. For further optimization of the tuner, the illustrated problem of ambiguous assignment could be used to improve the degree of matching during the tuning for known VSWR value and tuner parameters read off motors step positions. The modulated electro-hyperthermia (mEHT) is devoted to this particular task. The challenge involves an accurate matching to provide the energy from the source to the patient, allowing the conventional energy-dose, the same concept as the ionizing radiation applies. The uncontrolled energy loss makes the energy-based dosing of the treatment impossible. The adequately matched circuit promotes the selection mechanisms, and the energy is provided to the membrane rafts of the malignant cells causing immunogenic cell death. This type of cellular process gently liberates the genetic information of the malignant cells, which could be used for antigene presenting and promote building up a tumor-specific systemic immune reaction. This paper showed a beneficial opportunity to assess the suitability of a present adjustable passive impedance matching network in a mathematical way. Consequently, the proper matching optimized the electromagnetic effect on the selected cells and made possible the abscopal effect through the immune-modification.

References

[1] Sebastian M., Ninan N., Elias E. (2012) Nanomedicine and Cancer Therapies. Apple Academic Press
[2] Lee S-Y, Szigeti GP, Szasz AM. (2019) Oncological hyperthermia: The correct dosing in clinical applications, Int. J. Oncology, 54: 627-643
[3] Szasz A., Szasz N., Szasz O. (2011) Oncothermia: Principles and Practices. Springer Verlag
[4] Sokal NO. (2003) Class-E high-efficiency RF/microwave power amplifiers: Principles of operation, design procedures, and experimental verification, Analog Circuit Design, Springer, Boston MA, https://doi.org/10.1007/0-306-47950-8_14, pp. 269-301
[5] Li R.C.H. (2012) RF Circuit Design, 2nd Edition. John Wiley & Sons, Hoboken, New Jersey
[6] Misra K.M. (2004) Radio - Frequency and Microwave Communication Circuits: Analysis and Design, 2nd Edition. John Wiley & Sons, Hoboken, New Jersey
[7] Davis W.A. (2011) Radio Frequency Circuit Design, 2nd Edition. John Wiley & Sons, Hoboken, New Jersey
[8] Simonyi, K. (1965). Theoretische Elektrotechnik, VEB Verlag Berlin, 7th ed. 1979
[9] MATLAB R2008b. The MathWorks. Computer software
[10] Serenade v8.7. Ansoft Corporation. Computer software
[11] Breed G. (2007) There's Nothing Magic About 50 Ohms. High Frequency Electronics, pp. 6–7, June 2007, Summit Technical Media LLC.
[12] McCoy, Lewis G. (W1ICP) (July 1970). "Ultimate transmatch". QST Magazine. Newington, CT: American Radio Relay League. pp. 24–27, 58
[13] Qin W, Akutsu Y, Andocs G, et al. (2014) Modulated electro-hyperthermia enhances dendritic cell therapy through an abscopal effect in mice. Oncol Rep 32(6):2373-2379, http://www.ncbi.nlm.nih.gov/pubmed/25242303
[14] Hegyi G, Szigeti GP, Szasz A. (2013) Hyperthermia versus oncothermia: Cellular effects in complementary cancer therapy. Evid Based Complement Alternat Med 2013:672873
[15] Szasz A. (2013) Challenges and Solutions in Oncological Hyperthermia. Thermal Med 29(1):1-23
[16] Warburg O (1956) On the origin of cancer cells. Science 123(3191):309-314
[17] Warburg O (1996) Oxygen, The Creator of Differentiation, Biochemical Energetics. Academic Press, New York In: Warburg O (1996) The Prime Cause and Prevention of Cancer. Revised lecture at the meeting of the Nobel-Laureates on June 30, 1966, Lindau, Lake Constance, Germany
[18] Alfarouk KO, Shayoub MEA, Muddathir AK, Elhassan GO, Bashir AHH; (2011) Evolution of tumour metabolism might reflect carcinogenesis as a reverse evolution process (dismantling of multicellularity), Cancers 3:3002-3017
[19] Szigeti GP, Szasz O, Hegyi G. (2017) Connections between Warburg's and Szentgyorgyi's Approach about the Causes of Cancer. Journal of Neoplasm 1(2:8):1-13
[20] Grant JP; (1984), Measurements, Medical Significance And Applications Of The Dielectric Properties Of Biological Materials; PhD Thesis University of Surrey
[21] Mikac U, Demsar F, Beravs K, Sersa I. (2001) Magnetic resonance imaging of alternating electric currents, Magn Reason Imaging, 19:845-856
[22] Haemmerich D, Staelin ST, Tsai JZ, et al. (2003) In vivo electrical conductivity of hepatic tumors, Physiol. Meas. 24:251-260
[23] Smith SR, Foster KR, Wolf GL, (1986) Dielectric Properties of VX-2 Carcinoma Versus Normal Liver Tissue, IEEE Trans. On Biomed. Eng.; BME-33:522525
[24] Muftuler LT, Hamamura MJ, Birgul O, Nalcioglu O. (2006) In vivo MRI electrical impedance tomography (MERIT) of tumors, Technol Cancer Res Treat. 5:381-387
[25] Surowiec AJ, Stuchly SS, Barr JR, Swarup A. (1988) Dielectric properties of breast carcinoma and the surrounding tissues, IEEE Transactions on Biomedical Engineering, 35(4):257-263
[26] Chaudhary S, Mishra R, Swarup A, Thomas JM. (1984) Dielectric properties of normal and malignant human breast tissues at radiowave and microwave frequencies, Indian J Biochem Biophys. 21:76-79
[27] Scholz B, Anderson R. (2000) On electrical impedance scanning – principles and simulations, Electromedica Onco, 68:35-44
[28] Sha L, Ward ER, Story B. (2002) A Review of Dielectric Properties of Normal and Malignant Breast Tissue; Proceedings IEEE Southeastcon, pp.457-463, DOI: 10.1109/SECON.2002.995639
[29] Chaudharyet. al, (1984) Dielectric properties of normal and malignant human breast tissues, Indian J. Biochem. Biophys., 21:76-79

[30] Cole KS. Cole RH. (1941) Dispersion and Absorption in Dielectrics I. Alternating Current Characteristics, Journal of Chemical Physics. 9:341–351
[31] Ivorra A. (2002) Bioimpedance Monitoring for physicians:an overview, Centre Nacional de Microelectrònica Biomedical Applications Group, https://www.researchgate.net/publication/253563215_Bioimpedance_Monitoring_for_physicians_an_overview
[32] Kalmykov YP; Coffey WT; Crothers DSF; Titov SV. (2004) Microscopic Models for Dielectric Relaxation in Disordered Systems, Physical Review E. 70:041103
[33] Salengke S, Sastry SK. (2007) Experimental investigation of ohmic heating of solid–liquid mixtures under worst-case heating scenarios, Journal of Food Engineering, 83:324-336
[34] Nelson SO, Charity LF. (1972) Frequency dependence of energy absorption by insects and grain in electric fields. Transactions of the ASAE 15:1099-1102
[35] Schwan, H.P. Mechanism responsible for electrical properties of tissues and cell suspensions. Med. Prog. Technol. 1993, 19, 163–165
[36] Nasir N, Al-Ahmad M, (2020) Cells Electrical Characterization: Dielectric Properties, Mixture, and Modeling Theories, Hindawi Journal of Engineering, Volume 2020, Article ID 9475490, 17 pages, https://doi.org/10.1155/2020/9475490
[37] Stubbe M, Gimsa J, (2015) Maxwell's Mixing Equation Revisited: Characteristic Impedance Equations for Ellipsoidal Cells, Biophysical Journal 109:194–208
[38] Cole, K.S. Membranes, Ions and Impulses; University of California Press: Berkeley, 1972
[39] Anderson JC. (1964) Dielectrics, Chapman & Hall, London
[40] Pethig RR. (1979) Dielectric and Electronic Properties of Biological Materials; Wiley
[41] Schwan, HP. (1957) Advances in Biological and Medical Physics, 5:147
[42] Martinsen Ø G, Grimnes S and Mirtaheri P (2000): Non-ivasive measurements of post mortem changes in dielectric properties of haddock muscle - a pilot study. J. Food Eng. 43:189-192
[43] Grant EH, Sheppard RJ, South SP. (1978) Dielectric behavior of biological molecules in solution; Clarendon Press, https://doi.org/10.1016/0307-4412(79)90015-3
[44] Schwarz G. Seelig J. (1968) Kinetic properties and the electric field effect of life helix-coil transition of poly(γ-benzyl L-glutamate) determined from dielectric relaxation measurements, Biopolymers, 6:1263, 1263-1277
[45] Debye and Falkenhagen (1928) Dispersion of the conductivity and dielectric constants of strong electrolytes, Phys. Z. 29:121-401
[46] Pethig RR, (2017) Dielectrophoresis: Theory, Methodology and Biological Applications, John Wiley & Sons, Hoboken, NJ, USA, 2017
[47] Asami K, (2002) Characterization of biological cells by dielectric spectroscopy, Journal of Non-crystalline Solids, 305:268–277
[48] Pauly, H.; Schwan, H.P. Uber die Impedanz einer Suspension von Kugelformigen Teilchen mit einer Schale. Z. Naturforsch., B 1959, 14B, 125–131
[49] Stoy, R.D.; Foster, K.R.; Schwan, H.P. Dielectric properties of mammalian tissues from 0.1 to 100 MHz: a summary of recent data. Phys. Med. Biol. 1982, 27, 501–513
[50] Gotz M, Karsch L, Pawelke J, (2017) A new model for volume recombination in plane-parallel chambers in pulsed fields of high dose-per-pulse, Physics in Medicine & Biology, 62:8634–8654
[51] Szasz O, Szasz A.M. Minnaar C, Szasz A (2017) Heating preciosity - trends in modern oncological hyperthermia. Open Journal of Biophysics 7:116-144
[52] Pethig R: Dielectric properties of biological materials: biophysical and medical application. IEEE Transactions on Electrical Insulation, E1-19(5),453-474, 1984
[53] Schwan HP: Determination of biological impedances. In: Physical Techniques in Biological Research, vol. 6, 323-406, Academic Press, New York, 1963
[54] Szasz O and Szasz A: Oncothermia - nano-heating paradigm. J Cancer Sci Ther, 6:4, 2014
[55] Vincze Gy, Szigeti Gy., Andocs G and Szasz A: Nanoheating without artificial nanoparticles. Biology and Medicine, 7(4),249, 2015
[56] Szasz A: Electromagnetic effects in nanoscale range. Cellular Response to Physical Stress and Therapeutic Applications (eds. Tadamichi Shimizu, Takashi Kondo), chapter 4, Nova Science Publishers, Inc, 2013
[57] Martinsen OG, Grimnes S, Schwan HP; (2002) Interface Phenomena and Dielectric Properties of Biological Tissue; Encyclopedia of Surface and Colloid Science; pp. 2643-2652, Marcel Dekker, Inc.

[58] Ayoub MWB, Aro R, Georgin E, et al. (2018) Quantification of free and bound water in selected materials using dielectric and thermo-coulometric measurement methods; J. Phys. Commun. 2:035040
[59] Wolf M, Gulich R, Lunkenheimer P, Loidl A. (2012) Relaxation dynamics of a protein solution investigated by dielectric spectroscopy, Biochimica et Biophysica Acta - Proteins and Proteomics 2012
[60] Hasted JB. Aqueous dielectrics, Chapman and Hall, London, Ch.9, pp.234-256, 1973
[61] Andocs G, Renner H, Balogh L, Fonyad L, Jakab C, Szasz A. (2009) Strong synergy of heat and modulated electro- magnetic field in tumor cell killing, Study of HT29 xenograft tumors in a nude mice model. Strahlentherapie und Onkologie 185:120–126, http://www.ncbi.nlm.nih.gov/pubmed/19240999
[62] Szasz A, Vincze G, Szasz O, Szasz N. (2003) An energy analysis of extracellular hyperthermia. Magneto- and electro-biology 22:103-115
[63] Lee I-H, Imanaka MY, Modahl EH, et.al. (2019) Lipid raft phase modulation by membrane-anchored proteins with inherent phase separation properties, ACS Omega, 4, 6551-6559
[64] Staunton JR, Wirtz D, Tlsty TD, et al, The Physical Sciences - Oncology Centers Network; (2008) A physical sciences network characterization of non-tumorigenic and metastatic cells; Scientific Reports, 3:1449, https://doi.org/10.1038/srep01449
[65] Kotnik, T., (2000) Theoretical Evaluation of the Distributed Power Dissipation in Biological Cells Exposed to Electric Fields. Bioelectromagnetics, 21, 385–394.
[66] Campello, E.M.B. and Zohdi, T.I. (2014) Design Evaluation of a Particle Bombardment System Used to Deliver Substances into Cells. CMES, 98(2), 221–245.
[67] Lee, B.W., Faller, R., Sum, A.K., Vattulainen, I., Patra, M. and Karttunen, M. (2004) Structural Effects of Small Molecules on Phospholipid Bilayers Investigated by Molecular Simulations. Fluid Phase Equilib, 225, 63-8.
[68] Guest, W.C., Cashman, N.R. and Plotkin, S.S. (2011) A theory for the anisotropic and inhomogeneous dielectric properties of proteins. Phys Chem Chem Phys ,13(13), 6286–95.
[69] Heikelä, M., Vattulainen, I. and Hyvönen, M.T. (2006) Atomistic simulation studies of cholesteryl oleates: model for the core of lipoprotein particles. J Biophys, 90(7), 2247–57.
[70] Waxham, M.N. (2007) Molecular mobility in cells examined with optical methods. Bean A. Protein Trafficking Neurons, 3-27.
[71] Meggyeshazi N, Andocs G, Krenacs T. (2013) Programmed cell death induced by modulated electro-hyperthermia. Hindawi Publishing Corporation Conference Papers in Medicine, Volume 2013, Article ID 187835, http://www.hindawi.com/archive/2013/187835/
[72] Forika G, Balogh A, Vancsik T, Zalatnai A, et.al. (2020) Modulated electro-hyperthermia resolves radioresistance of Panc1 pancreas adenocarcinoma and promotes DNA damage and apoptosis in vitro, Int. J. Mol. Sci., 21, 5100, 1-15, https://pubmed.ncbi.nlm.nih.gov/32707717/
[73] Kao P H-J, Chen C-H, Chang Y-W, et al. (2020) Relationship between energy dosage and apoptotic cell death by modulated electro-hyperthermia, Scientific reports, 10:8936, DOI: 10.1038/s41598-020-65823-2, https://www.nature.com/articles/s41598-020-65823-2
[74] Veatch SL, Cicuta P, Sengupta P, Honerkamp-Smith A, Holowka D, Baird B; (2008) Critical Fluctuations in Plasma Membrane Vesicles; ACS Chem.Biol. 3:287-295
[75] Zalba S, ten Hagen TLM, (2017) Cell membrane modulation as adjuvant in cancer therapy; Cancer Treatment Rev. 52:48-57
[76] Dietrich C, Bagatolli LA, Volovyk ZN, et.al. (2001) Lipid rafts reconstituted in model membranes, Biophysical Journal, 80: 1417-1428
[77] Dewey WC. (1993) Arrhenius relationships from the molecule and cell to the clinic, Int J Hyperthermia, 25:1, 3-20, DOI: 10.1080/02656730902747919
[78] Feo F, Canuto RA, Garcea R. (1976) Lipid phase transition and breaks in the Arrhenius plots of membrane-bound enzymes in mithochondria from normal rat liver and hepatoma AH-130, FEBS Letters, 7(2): 262-266
[79] Pelzer, H., Wigner, E.: Uber die Geschwindigkeitskonstante von Austauschreaktionen. Z. Phys. Chem. B15, 445–471 (1932)
[80] Eyring, H.: The Activated Complex in Chemical Reactions. J. Chem. Phys. 3, 107-115 (1935)
[81] Laidler, K.J., King, M.C.: The development of transition-state theory. J. Phys. Chem. 87, 2657-2664 (1983)
[82] Miller WH (1993) Beyond transition-state theory: a rigorous quantum theory of chemical reaction rates. Acc Chem Res 26:174-181

[83] Pollak E, Talkner P (2005) Reactio rate theory: what it was, where is it today, and where is it going? Chaos 15(2):26116-26117
[84] Szasz A, Vincze Gy (2006) Dose concept of oncological hyperthermia: Heat-equation considering the cell destruction. Journal of Cancer Research and Therapeutics 2(4):171-181
[85] O'Neil DP, Peng T, Stiegler P, et al. (2011) A three-state mathematical model of hyperthermic cell death, Ann. Biom. Eng. 39(1):570-579
[86] Pearce JA. (2013) Comparative analysis of mathematical models of cell death and thermal damage processes, Int. J. Hyp. 29(4): 262-280
[87] Vincze Gy, Szasz A. (2018) Similarities of modulation by temperature and by electric field, OJBIPHY, 8, 95-103, https://www.scirp.org/journal/PaperInformation.aspx?PaperID=84883
[88] Szasz O, Szasz A. (2014) Oncothermia - Nano-heating paradigm. J Cancer Sci Ther 6:4
[89] Papp E, Vancsik T, Kiss E, Szasz O. (2017) Energy absorption by the membrane rafts in the modulated electro-hyperthermia (mEHT), Open Journal of Biophysics, 7, 216-229
[90] Megyesshazi N. (2015) Studies on modulated electrohyperthermia induced tumor cell death in a colorectal carcinoma model, Ph.D. theses, Pathological Sciences Doctoral School, Semmelweis University
[91] Krenacs T, Meggyeshazi N, Forika G, et.al. (2020) Modulated electro-hyperthermia-induced tumor damage mechanisms revealed in cancer models, Int J Molecular Sciences, 21, 6270, pp. 1-25, doi:10.3390/ijms21176270
[92] Vancsik T, Forika G, Balogh A, et.al. (2019) Modulated electro-hyperthermia induced p53 driven apoptosis and cell cycle arrest additively support doxorubicin chemotherapy of colorectal cancer in vitro, Cancer Medicine, (9):4292-4303, doi: 10.1002/cam4.2330, https://www.ncbi.nlm.nih.gov/pubmed/31183995
[93] Yang K-L, Huang C-C, Chi M-S, Chiang H-C, Wang Y-S, Andocs G, et.al. (2016) In vitro comparison of conventional hyperthermia and modulated electro-hyperthermia, Oncotarget, 7(51): 84082-84092, doi: 10.18632/oncotarget.11444, http://www.ncbi.nlm.nih.gov/pubmed/27556507
[94] Andocs G, Rehman MU, Zhao Q-L, Tabuchi Y, Kanamori M, Kondo T. (2016) Comparison of biological effects of modulated electro-hyperthermia and conventional heat treatment in human lymphoma U937 cell, Cell Death Discovery (Nature Publishing Group), 2, 16039, http://www.nature.com/articles/cddiscovery201639
[95] Szasz A, Szasz O. (2020) Time-fractal modulation of modulated electro-hyperthermia (mEHT), in book Challenges and solutions of oncological hyperthermia, ed. Szasz A., Ch. 17, pp.377-415, Cambridge Scholars
[96] Wust P, Kortum B, Strauss U, Nadobny J, Zschaeck S, Beck M, et.al. (2020) Nonthermal effects of radiofrequency electromagnetic fields, Scientific Reports, 10:13488
[97] Wust P, Ghadjar P, Nadobny J, et.al. (2019) Physical analysis of temperature-dependent effects of amplitude-modulated electromagnetic hyperthermia, Int. J. Hyp., 36(1):1246-1254
[98] Wust P, Nadobny J, Zschaeck S, Ghadjar P. (2020) Physics of hyperthermia – Is physics really against us?, in book Challenges and solutions of oncological hyperthermia, ed. Szasz A., Ch. 16, pp.346-376, Cambridge Scholars
[99] Szasz A. (2019) Thermal and nonthermal effects of radiofrequency on living state and applications as an adjuvant with radiation therapy, Journal of Radiation and Cancer Research, 10:1-17
[100] Meggyeshazi N, Andocs G, Balogh L, Balla P, Kiszner G, Teleki I, Jeney A, Krenacs T (2014) DNA fragmentation and caspase-independent programmed cell death by modulated electrohyperthermia. Strahlenther Onkol 190:815-822
[101] Szasz A. (2020) Towards the immunogenic hyperthermic action: Modulated electro-hyperthermia, Clinical Oncology and Research, Science Repository, 3(9):5-6
[102] Andocs G, Meggyeshazi N, Balogh L, Spisak S, Maros ME, Balla P, Kiszner G, Teleki I, Kovago Cs, Krenacs T (2014) Upregulation of heat shock proteins and the promotion of damage-associated molecular pattern signals in a colorectal cancer model by modualted electrohyperthermia. Cell Stress and Chaperones 20(1):37-46
[103] Tsang Y-W, Huang C-C, Yang K-L, et al. (2015) Improving immunological tumor microenvironment using electro-hyperthermia followed by dendritic cell immunotherapy, BMC Cancer 15:708
[104] Szasz O. (2020) Local treatment with systemic effect: Abscopal outcome, in book Challenges and solutions of oncological hyperthermia, ed. Szasz A., Ch. 11, pp.192-205, Cambridge Scholars
[105] Vancsik T., Kiss E, Kovago Cs, Meggyeshazi N, Forika G, Krenacs T. (2017) Inhibition of proliferation, induction of apoptotic cell death and immune response by modulated electro-hyperthermia in C26 colorectal cancer allografts, thermometry Oncothermia Journal Volume 20: 277-292

[106] Minnaar CA, Kotzen JA, Ayeni OA, et al. (2020) Potentiation of the abscopal effect by modulated electro-hyperthermia in locally advanced cervical cancer patients, Frontiers in Oncology, 10(376):1-8
[107] Lee S-Y, Fiorentini G, Szasz AM, Szigeti Gy, Szasz A, Minnaar CA. (2020) Quo vadis oncological hyperthermia (2020)? Frontiers in Oncology, 10:1690, doi: 10.3389/fonc.2020.01690